Causes of Differences in Depiction of Convective Lines in 1-km and 3-km CM1 Simulations

SAMUEL T. LUTHI[a] AND WILLIAM A. GALLUS JR.[a]

[a] *Department of Geological and Atmospheric Sciences, Iowa State University, Ames, Iowa*

(Manuscript received 27 October 2023, in final form 24 October 2024, accepted 2 December 2024)

ABSTRACT: Previous research has shown that 3-km horizontal grid spacing simulations depicting clusters of cells often change to showing linear structures when grid spacing is refined to 1 km. This increase in linear structures at finer horizontal grid spacings may be due simply to the resolving of stronger vertical motion along the leading edge of the MCS cold pool resulting in more continuous zones of convection in higher-resolution runs. However, prior work has suggested that the cold pools themselves are stronger with finer grid spacing, enhancing lift to grow linear morphologies faster. In the present study, Cloud Model 1 was used to simulate an array of MCSs with varying wind profiles and a constant thermodynamic profile (Weisman–Klemp analytic sounding) at both 1- and 3-km horizontal grid spacings and with 50 and 100 vertical levels. A line of seven randomly spaced warm bubbles was used to initiate convection. In 1-km Δx simulations, gravity waves dominated in initiating new convection for growth into lines, and the ascent associated with them was much greater than in 3-km runs. Upscale growth into lines in 3-km Δx simulations was driven more by ascent caused by the collision of convective cold pools.

KEYWORDS: Convection lines; Mesoscale forecasting; Idealized models; Numerical weather prediction/forecasting

1. Introduction

Mesoscale convective systems (hereafter MCSs) are a significant meteorological phenomenon in the Great Plains region of the United States given that these large collections of thunderstorms are estimated to account for between 30% and 70% of the total warm season precipitation there (e.g., Fritsch et al. 1986; Ashley et al. 2003; Haberlie and Ashley 2019). While such rainfall is essential to the agriculture industry, MCSs also present a variety of meteorological hazards, such as severe winds, hail, flash flooding, and tornadoes (e.g., Maddox 1980; Maddox et al. 1982; Junker et al. 1999; Gallus et al. 2008; French and Parker 2012). MCS hazards are particularly dangerous to the public since the majority of MCSs are nocturnal (e.g., Carbone and Tuttle 2008; Geerts et al. 2017), when public alertness and preparedness are at a minimum (e.g., Haberlie and Ashley 2019). Given both the necessity and danger of these systems, accurate forecasting of MCSs is critical.

Despite historical difficulty in forecasting MCSs (e.g., Stensrud and Fritsch 1994; Jirak and Cotton 2007; Coniglio et al. 2010; Squitieri and Gallus 2016), forecasts for these complexes of thunderstorms have significantly improved, most notably through the use of convection-allowing models (CAMs) (e.g., Done et al. 2004; Weisman et al. 2008; Clark et al. 2010a,b, 2011; Gallo et al. 2017). It has been found in some studies that continued refinement of horizontal grid spacing (denoted as Δx later in this paper) in CAMs leads to improved MCS forecast accuracy, including improvements in precipitation forecasts and general MCS structure (e.g., Schwartz et al. 2017; Weisman et al. 2023), although some questions remain over whether the improvements found using grid spacings as fine as 1 or 2 km are worth the increased computational cost. Schwartz and Sobash (2019), for instance, found that although precipitation forecasts generally improved as Δx was refined from 3 to 1 km, the improvement was most notable in the cool parts of the year in cases where synoptic forcing was strong. During the summer when forcing for convection was weakest, little improvement occurred; this is important when considering the fact that MCSs and their associated precipitation are more prevalent during the summer months. On the other hand, it has been postulated that refinement of Δx to values less than 250 m may be needed to properly capture deep convective processes (Bryan et al. 2003).

The refinement of Δx to even smaller values than have been traditionally used in both many prior MCS modeling studies and current operational CAM runs, such as 3 or 4 km, may be particularly important to accurately resolve vertical motion along the leading edge of the MCS. This is hypothesized given the research that has shown that vertical motion is highly dependent on Δx (Weisman et al. 1997) and that the vertical motion in this region may play a critical role in determining convective morphology and its evolution. This decrease in Δx in MCS simulations to values below 3 or 4 km has been found to support stronger and more numerous updrafts (e.g., Bryan and Morrison 2012). Prior research has shown that 3-km Δx tends to capture cellular systems better than linear ones, in some cases overpredicting them, while underpredicting linear systems, most notably bow echoes and lines with trailing stratiform precipitation (e.g., Snively and Gallus 2014; Carlberg et al. 2018; Thielen and Gallus 2019). Although the reduction in Δx from 3 to 1 km has been found to increase the proportion of simulated linear systems to cellular systems, better matching the ratio observed, a morphology accuracy score (Snively and Gallus 2014) did not show any statistically significant improvement (Thielen and Gallus 2019) from the change. This suggests there may be problems with the timing of the linear phase of systems or the formation

Corresponding author: Samuel T. Luthi, stluthi@iastate.edu

DOI: 10.1175/MWR-D-23-0240.1

and position of stratiform rain relative to the convective line. In addition, a more recent study by Weisman et al. (2023) indicated that although simulations using 1-km horizontal grid spacing did better define the general leading line-trailing stratiform region structure in squall lines, both grid spacings were able to reproduce bow echo and line echo wave patterns in the systems.

Thunderstorm cold pools play an important role in the upscale convective growth and morphological evolution of MCSs as well (e.g., Rotunno et al. 1988; Coniglio and Stensrud 2001; James et al. 2005; Bryan and Morrison 2012; Hiris and Gallus 2021; Parker et al. 2020; Parker 2021; Weisman et al. 2023). Even initially elevated systems being maintained dynamically by wavelike disturbances can mature into systems that are partially surface based. These systems are then maintained and organized via surface cold pools, implying that these systems may not be reliant on larger-scale features external to the convection (Parker et al. 2020; Parker 2021). MCS cold pools have been found to be significantly larger in areal coverage in runs that use 1-km grid spacing instead of 3 km, but cold pools in simulation where Δx is decreased further to below 1 km display less pronounced changes in magnitude, depth, length, and areal coverage (Squitieri and Gallus 2020). These stronger, more robust cold pools in 1 km and finer runs have been shown to potentially be the result of stronger and more abundant updrafts located on the leading edge of the MCS, which would loft a greater mass of hydrometeors rearward, enhancing latent cooling and thus strengthening the cold pool in a positive feedback loop (Squitieri and Gallus 2022a). The Squitieri and Gallus (2022a) study simulated 11 MCS events with the WRF Model, using both 1- and 3-km Δx, and 50 and 100 vertical levels, and focused on the impacts of resolution changes on several cold pool characteristics and the microphysical processes that contributed to the changes. It was found that 3-km simulations with 100 vertical levels produced the deepest cold pools, while 1-km simulations produced cold pools with larger areal coverage caused by stronger and more numerous updrafts along the leading edge of the MCS. These updrafts were found to be potent in advecting greater amounts of hydrometeors rearward and, as a result, increasing the latent cooling at lower levels.

Adams-Selin (2020a) has shown that convectively generated gravity waves also may play a role in the evolution and maintenance of MCSs, where the generation of waves leads to environmental destabilization, strengthening updrafts, and developing cells to maintain the MCS. Tests involving the sensitivity of these gravity waves to variations in microphysics have demonstrated that such variations tend to not generate higher-order wave modes (where the wavenumber is greater than 2), but still cause different impacts in the effects of the waves, primarily in the development of discrete cells ahead of the convective line (Adams-Selin 2020b). Groff et al. (2021) have shown that the incorporation of deep vertical wind shear (as opposed to a weak, linear wind shear profile that decreased to 0 m s^{-1} by 5 km) leads to low-frequency waves from the MCS that can support and sustain both cloud development and convection ahead of the MCS.

The present research builds upon the findings of Squitieri and Gallus (2022a) to better understand the increase in linear events when Δx is decreased in numerical simulations and to determine what role changes in the depiction of cold pools in higher resolution runs may play in this increase in linear events. The use of an idealized, cloud-resolving model (CM1) allows more direct control over physical processes contributing to MCS morphology while avoiding the influences of terrain and unknown atmospheric heterogeneities that may influence and alter MCS evolution. More specifically, the present research explores whether the increase in linear structures at finer Δx is due to the resolution of stronger vertical motion alone due to finer grid spacing, either at the leading edge of the cold pool or within gravity waves. It also explores what roles changes in cold pools play by their effect in strengthening vertical motion along the leading edge of the MCS.

2. Data and methodology

a. CM1 setup—idealized cases

Community Cloud Model 1 (CM1, version 20.2) (Bryan and Fritsch 2002; Bryan et al. 2003) was used to perform idealized simulations of convection for the present study. Horizontal grid spacings of 3 and 1 km were used to investigate the impact of decreasing horizontal grid spacings on MCS morphology, upscale growth, and cold pool characteristics. CM1 was run on a stretched grid with both 50 and 100 vertical levels used, with the finer grid spacing being concentrated in the lowest 2–4 km. Adding the extra 50 vertical levels was done to determine the impact of the improved vertical resolution on processes involved in MCS development and evolution. The 50 levels were added by decreasing the vertical grid spacing by half at all elevations. For brevity, grid spacing configurations will be abbreviated as 3 km-50 lev, 3 km-100 lev, 1 km-50 lev, and 1 km-100 lev.

A 900 × 900 km^2 domain was employed to allow for the evolution of initial convection to be within lateral boundaries while not exceeding computational resources available for the study. Open boundary conditions for the lateral boundaries and a semislip condition for the bottom boundary were used. Runs were performed over a flat surface with no elevation changes to exclude terrain influences on convection. The model was run until 8 h after convective initiation, with results output half hourly. All runs employed the Thompson microphysical scheme (Thompson et al. 2008) and the Mellor–Yamada Janjic (MYJ) boundary layer parameterization (Janjić 1990, 1994; Janjić et al. 2001) to closely mirror past studies that similarly focused on grid spacing impacts on some aspects of MCSs (Squitieri and Gallus 2020, 2022a,b). The MYJ surface layer scheme was also employed in the model setup. No additional subgrid-scale mixing was considered beyond the MYJ PBL scheme. Surface fluxes of heat and moisture were included in the model. An upper-level Rayleigh damping zone was used and was damped toward the base state. A radiation scheme was not incorporated into the model setup due to computational constraints.

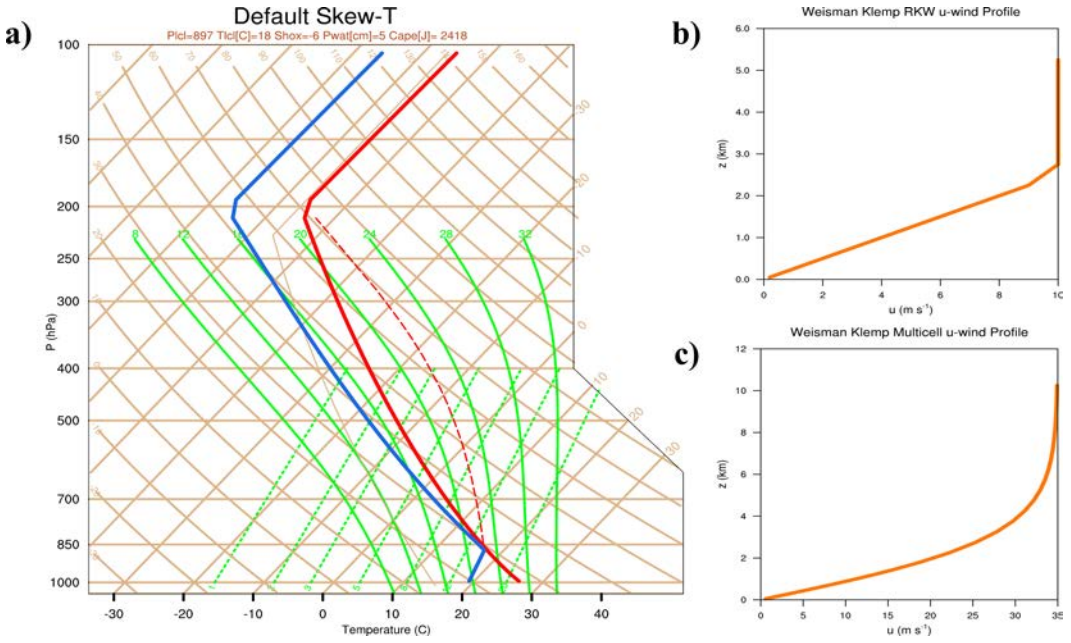

FIG. 1. CM1 environment vertical profiles using (a) Weisman and Klemp (1982) analytic thermodynamic sounding where the red line is temperature, the blue line is the dewpoint, and the dashed red line is the profile of a parcel lifted pseudoadiabatically from the surface, (b) Weisman–Klemp RKW u-wind profile, and (c) Weisman–Klemp MC u-wind profile.

All of the simulations used the Weisman–Klemp analytic thermodynamic sounding (Weisman and Klemp 1982) with two basic vertical wind profiles [Rotunno–Klemp–Weisman (RKW) u-wind profile and Weisman–Klemp multicell u-wind profile] as depicted in Fig. 1. These idealized environments allowed for the exploration of vertical wind shear impacts on cold pool evolution and upscale growth with changing horizontal and vertical grid spacings, while allowing for the exclusion of influences from changes in stability, baroclinicity, or terrain that could obfuscate analyses and conclusions. It should be noted that the Weisman–Klemp sounding has a greater moisture content than more typical profiles in the central United States.

To initialize convection in the CM1 runs, a line of seven randomly spaced warm bubbles was utilized. The line of bubbles was placed at the left edge of the domain to prevent the storm from prematurely leaving the domain before maturity. All bubbles were centered at a height of 1.4 km above the ground and had horizontal and vertical radii of 10 and 1.4 km, respectively. All bubbles had a maximum potential temperature perturbation of 5 K which worked well to cause rapid initiation of cells that developed upscale.

b. *Relevant equations and definitions*

Cold pool intensity was quantified using the cold pool parameter C, which represents the theoretical speed of a two-dimensional gravity current, which acts as a proxy for the cold pool (e.g., Rotunno et al. 1988; Weisman 1992). Weisman (1992) gives a generalized form of the equation for C:

$$C^2 = 2\int_0^H (-B)dz,$$

where z is the height above ground level, H is the height of the cold pool top, defined as the height where buoyancy first becomes positive, and B is the buoyancy, defined as

$$B \equiv g\left[\frac{\theta'}{\overline{\theta}} + 0.61(q_v - \overline{q}_v) - q_c - q_r - q_i\right],$$

where θ is the potential temperature, g is the acceleration due to gravity, and q_v, q_c, q_r, and q_i are the mixing ratios of water vapor, cloud water, rainwater, and ice (this includes all ice species: cloud ice, snow, graupel/hail), respectively. The term $\overline{q}_v$ represents the mean vapor mixing ratio. For all terms in the equation, overbars represent ambient values and primes represent deviations from the ambient value.

Gravity wave speed was quantified using the following equation from Groff et al. (2021):

$$v = \frac{ND}{n\pi},$$

TABLE 1. Theoretical range of gravity wave speeds found in the present study based on wavenumbers that were identified by Adams-Selin (2020a).

Wave number	Gravity wave speed (m s^{-1})
1	57.65–78.32
2	28.82–39.16
3	19.22–26.11

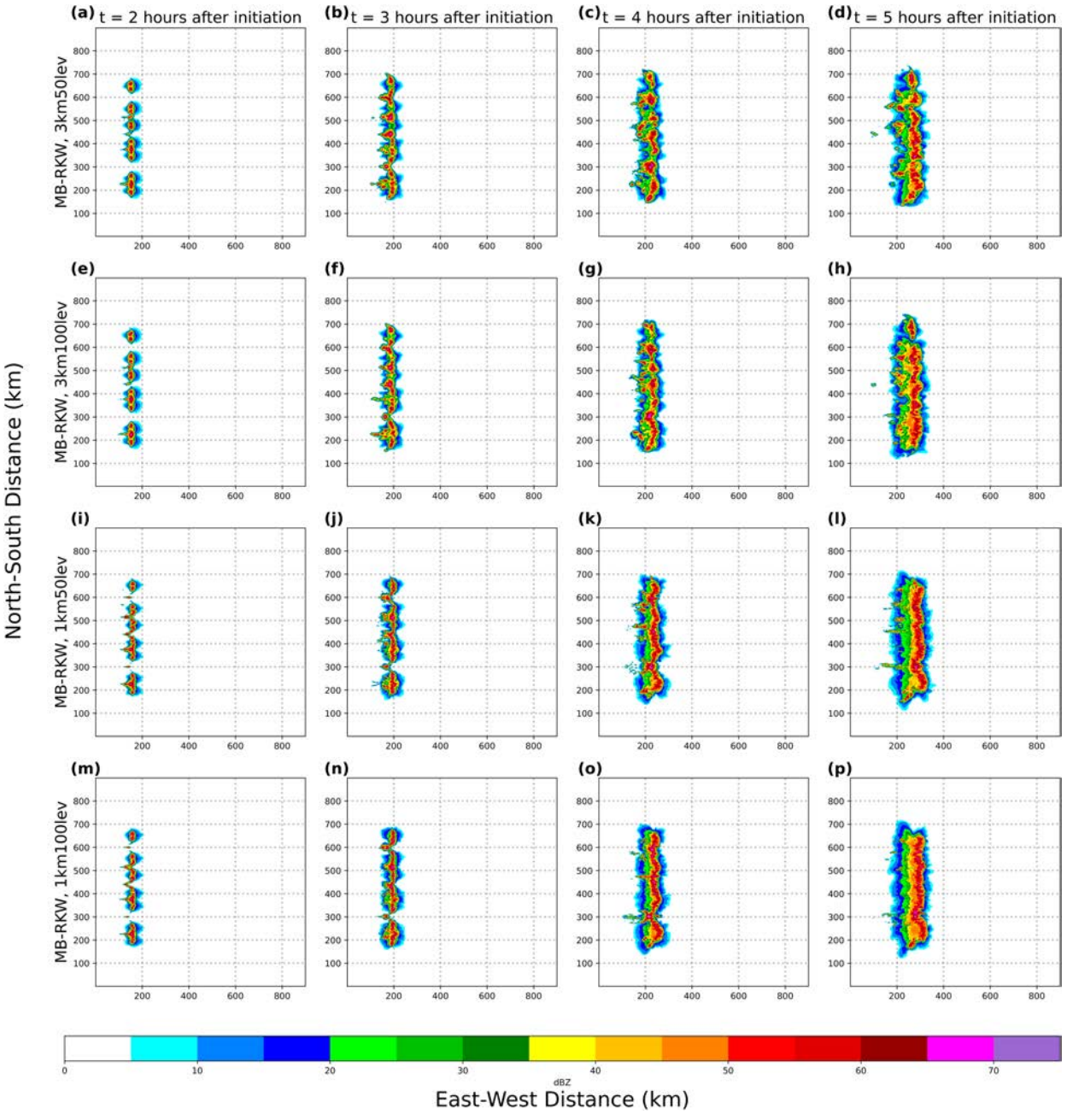

FIG. 2. Composite reflectivity of RKW MCSs for hours 2–5 for (a)–(d) 3 km-50 lev, (e)–(h) 3 km-100 lev, (i)–(l) 1 km-50 lev, and (m)–(p) 1 km-100 lev simulations.

with v being the gravity wave speed (m s^{-1}), N being the Brunt–Väisälä frequency (s^{-1}), D being the depth of the model simulation, and n being the vertical mode of the heating profile. The Brunt–Väisälä frequency was calculated using the following equation from Hobbs and Wallace (2006):

$$N = \left(\frac{g}{\theta}\frac{d\theta}{dz}\right)^{1/2},$$

where θ is the potential temperature. While virtual potential temperature is normally the relevant quantity, the potential temperature was used for simplicity; in doing so, moisture effects are ignored. Since the Brunt–Väisälä frequency is dependent on the stability, and thus dependent on the layer chosen, a range of frequencies in the 2–6-km layer for the hour that waves were most clearly visible were used to create a range of possible speeds at which theoretical gravity waves would travel based on their wavenumber at a height ranging from

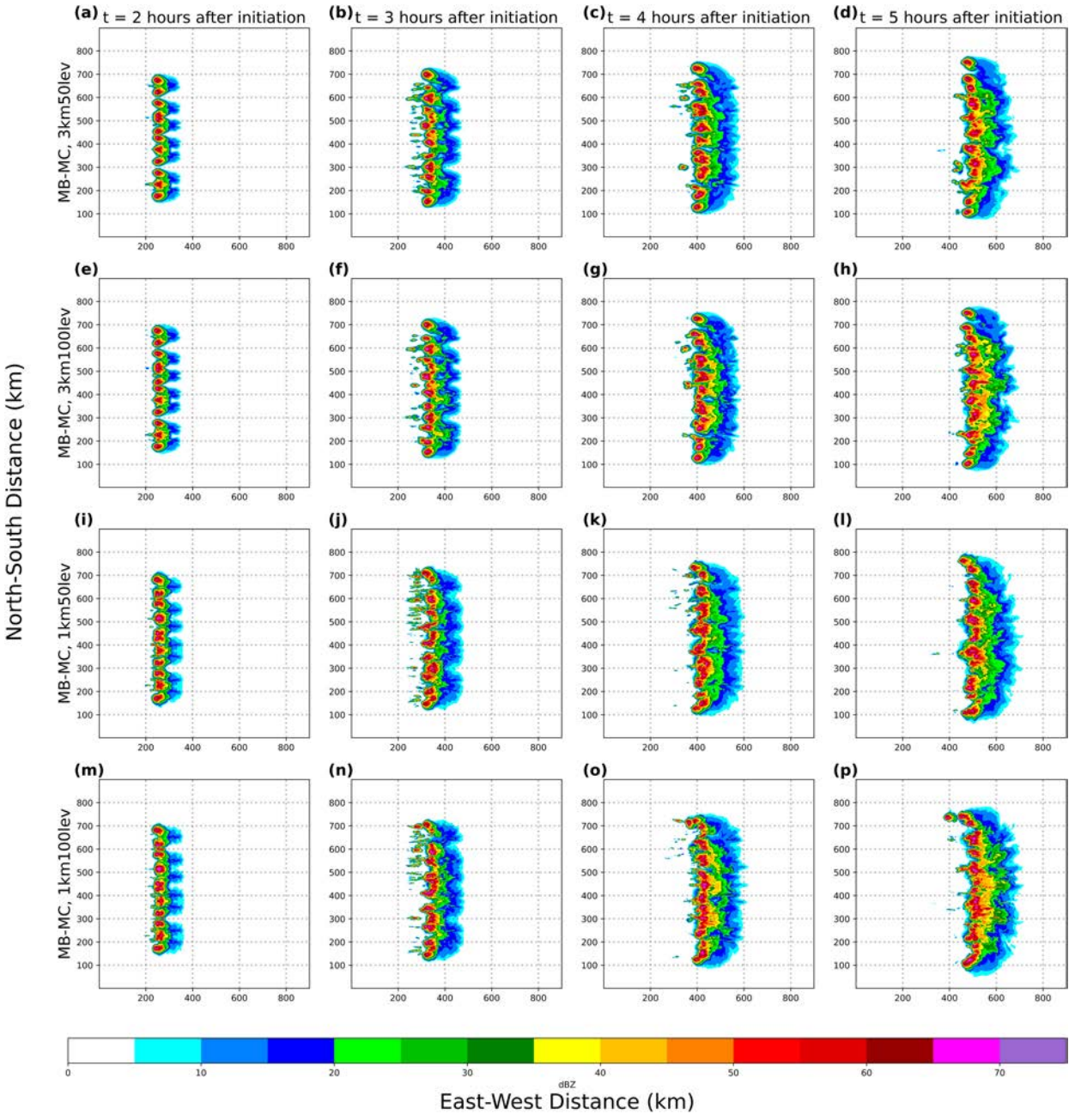

FIG. 3. Composite reflectivity of MC MCSs for hours 2–5 for (a)–(d) 3 km-50 lev, (e)–(h) 3 km-100 lev, (i)–(l) 1 km-50 lev, and (m)–(p) 1 km-100 lev simulations.

2 to 6 km. The range of Brunt–Väisälä frequencies was calculated using the vertical potential temperature gradients in this 2–6-km layer. This range of speeds is shown in Table 1. The wavenumbers listed were the wavenumbers that Adams-Selin (2020a) found identifiable in the model simulations performed in that study.

c. *Collection of bulk statistics*

An examination of the impact of coarsened versus uncoarsened data on bulk statistics was also performed. To allow for comparison with Squitieri and Gallus (2022b), 1-km datasets were regridded to 3 km, and datasets with 100 vertical levels were regridded to 50 vertical levels. Bulk statistics from data that were coarsened were also compared to the original 1-km output to determine the sensitivity and significance of the regridding. Additionally, for a given variable, values were excluded where composite reflectivity was less than 35 dBZ to allow for the collection of data from only the strongest portions of the MCSs. An examination of coarsened versus uncoarsened 1-km output showed no meaningful changes with

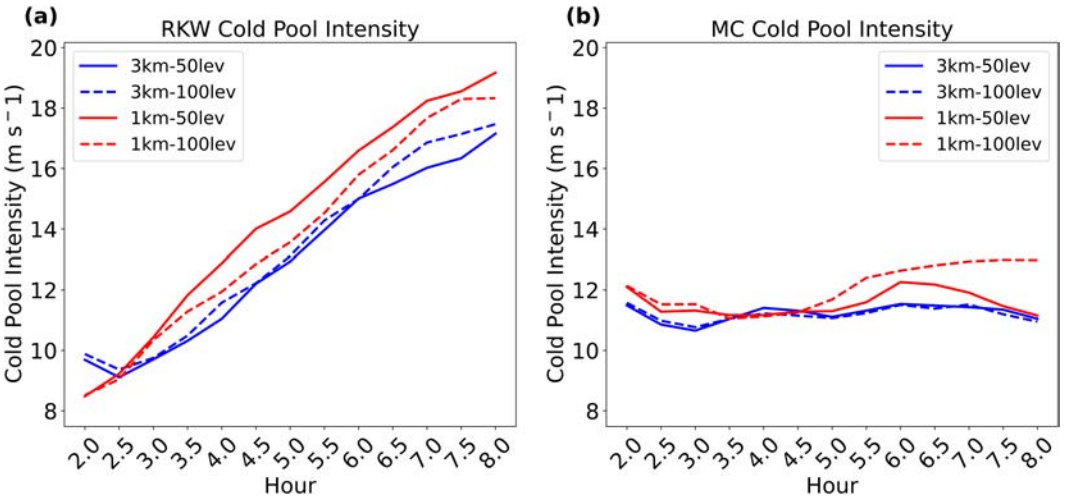

FIG. 4. Cold pool intensity magnitudes as a function of time after model initialization averaged over the area above the 75th percentile for (a) MB-RKW and (b) MB MC wind profile simulations.

respect to temporal trends or maximum and minimum magnitudes of bulk statistics (figures not shown).

Bulk statistics were generated for cold pool intensity and depth to examine how changes in model horizontal and vertical grid spacing may affect cold pool evolution and thus upscale convective growth into linear systems. For the calculation of bulk statistics, all values of a variable, such as cold pool intensity, for a given time were binned into a 1D array. The 75th percentile was then calculated based on this array; this percentile was chosen as it was determined to be representative of the stronger portions of cold pools, as in Squitieri and Gallus (2022b).

The time series of bulk statistics presented later was started at hour 2 so that values directly related to convective initiation from the artificial use of bubbles would not impact the analysis. It should be noted that although time-series figures use the coarsened data, all nontime series figures represent the noncoarsened data.

3. Results

a. *Qualitative comparison of CM1 MCSs*

MCSs produced by multibubble RKW wind profile (hereafter RKW) simulations took on linear structures by hour 5 (Fig. 2). Simulations with horizontal grid spacings of 3 km produced linear structures that were classified as broken lines (Figs. 2a–h). As horizontal grid spacings decreased to 1 km, the MCSs produced by RKW simulations appeared to be much more contiguous, with no breaks in the line (Figs. 2i–p). Additionally, 1-km lines appeared to have slightly greater areas of the most intense reflectivity (values of 60 dBZ and greater) in their mature stages than 3-km lines (Figs. 2d,h,l,p). It should also be noted that the

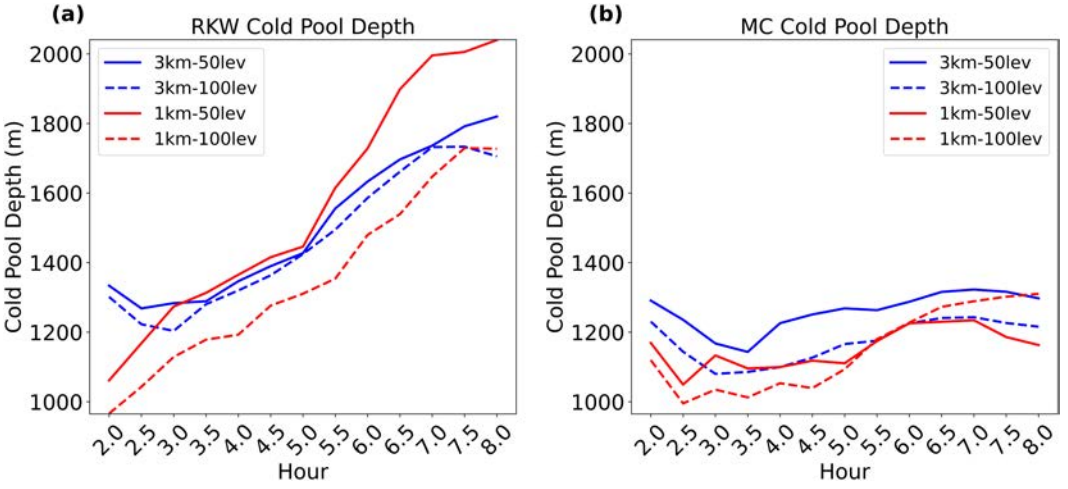

FIG. 5. Cold pool depth magnitudes as a function of time after model initialization averaged over the area above the 75th percentile for (a) MB-RKW and (b) MB MC wind profile simulations.

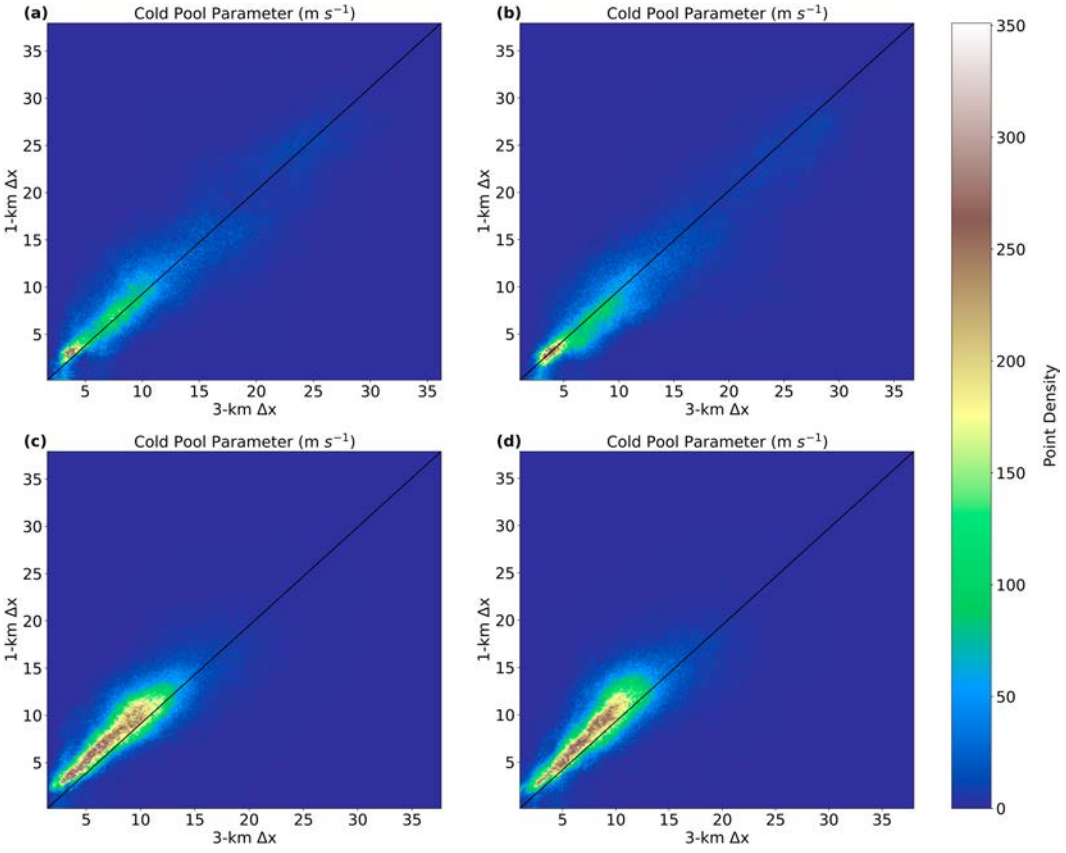

FIG. 6. Density heat maps (2D histograms) of cold pool intensity in MB (a),(b) RKW and (c),(d) MC simulations for both (a),(c) 50 and (b),(d) 100 vertical levels. Plotted data (see the scale on the right) are the aggregate of all hours of the simulations.

stratiform rain region of the MCSs for all configurations was located in the trailing portion of the system. Differences between MCS simulations with 50 and 100 vertical levels were minimal.

MCSs produced by multibubble multicell (MC) wind profile simulations had a much more broken appearance than the RKW MCSs (Fig. 3). Simulations with horizontal grid spacings of 3 km produced the most broken linear structures (Figs. 3a–h), while 1-km simulations produced MCSs with slightly more contiguous structures (Figs. 3i–p). As the number of vertical levels increased from 50 to 100, the linear structures became more cohesive when compared to the 50-level simulations (Figs. 3d,h,l,p), although this increased cohesion is rather subtle. Unlike MCSs produced by RKW simulations, MC MCSs had their stratiform rain regions located in the leading portion of the system. This is likely due to the strength of the Weisman–Klemp multicell u-wind profile.

b. *Cold-pool-associated bulk statistics*

As found in the WRF simulations of Squitieri and Gallus (2022b), surface cold pool intensities in the RKW CM1 simulations with different horizontal and vertical grid spacings followed similar overall temporal trends throughout the model run (Fig. 4a). RKW simulations with 3-km Δx had slightly stronger cold pools, based on the cold pool intensity C, in the 2–2.5-h range than the 1-km runs, but after this period, cold pools were stronger in the 1-km runs, although the differences in magnitudes between these simulations were only around 5%–10%. Two Wilcoxon–Mann–Whitney rank-sum tests were performed comparing the 3- and 1-km datasets to examine the significance regarding the 5%–10% difference in magnitudes. P values of 0.739 and 0.270 were found for comparisons between the 3 km-100 lev/1 km-100 lev and 3 km-50 lev/1 km-50 lev datasets, respectively, well above a significance threshold of 0.05. As a result, the difference in magnitudes was not found to be significant. Regardless of horizontal grid spacing or number of vertical levels, RKW simulations had steadily increasing cold pool intensities throughout the entire run as would be expected with an MCS that is growing upscale and reaching maturity. RKW simulations with grid configurations of 1 km-50 lev and 3 km-50 lev also produced deeper cold pools than their 100-level counterparts, with 1 km-50 lev simulations producing substantially deeper cold pools than all other configurations (depths of 1800 m and greater) (Fig. 5a).

A density heat map of the RKW and MC runs for all grid configurations was created; the 1-km data were regridded to 3 km to allow for fair comparison with the 3-km data. The plotted data show an aggregate of all hours for the simulations, and each count in the point density was from a single

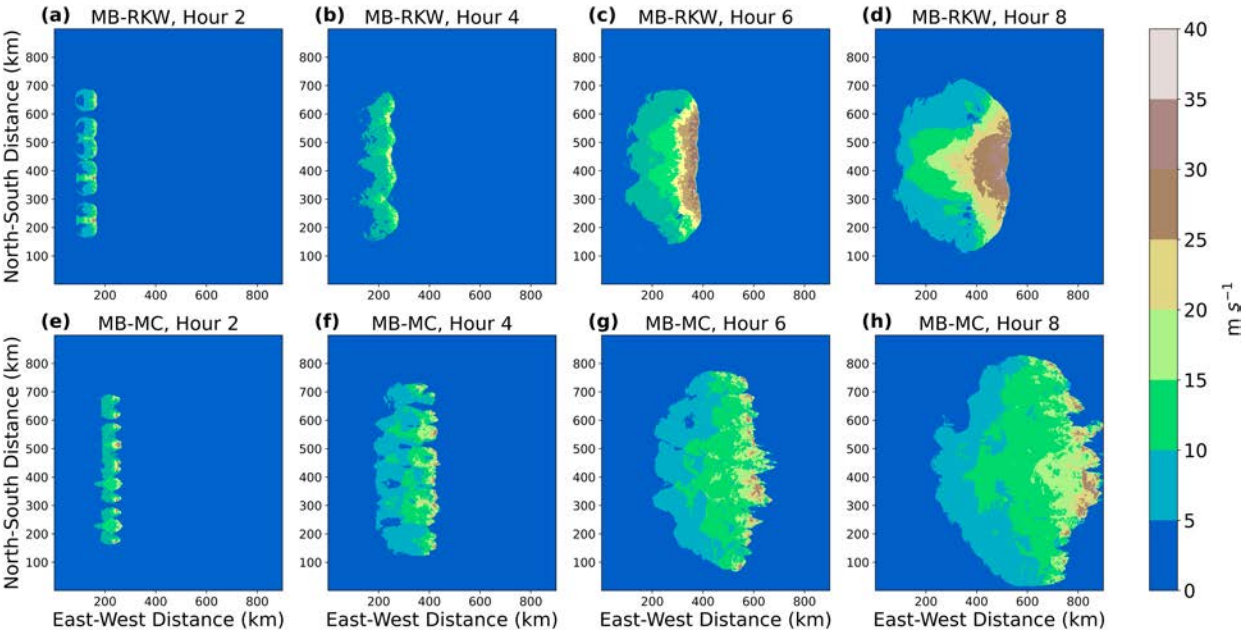

FIG. 7. Horizontal variations in cold pool parameter (see color bar on right; m s^{-1}) from hours 2–8 in 1 km-100 lev (a)–(d) RKW and (e)–(h) MC simulations.

output time and single grid cell. Density heat maps of cold pool intensities for the RKW simulations also showed that runs with 1-km Δx had slightly stronger cold pool intensities than simulations with 3-km Δx (Fig. 6a), especially when the number of vertical levels increased from 50 to 100. With the configuration using 50 vertical levels (Fig. 3a), cold pool strength rarely exceeded 5 m s^{-1} and cold pool intensity values exceeding 5 m s^{-1} did not change consistently as grid spacing changed from 3 to 1 km.

When vertical resolution was refined to use 100 vertical levels (Fig. 6b), cold pool strength exceeded 5 m s^{-1} more frequently, with a greater density of intensity values exceeding 5 m s^{-1} in 1-km runs compared to the 3-km run. This contrasts with Squitieri and Gallus (2022b) who found that cold pools were slightly more intense in simulations with 3-km Δx. However, Squitieri and Gallus (2022b) found that the cold pool intensity in 3- and 1-km runs did not differ significantly. The present study's finding that simulations with 100 vertical levels (Fig. 6b) produced cold pools of stronger intensities when compared to simulations with 50 vertical levels (Fig. 6a) was also found by Squitieri and Gallus (2022b).

MC simulations had far less pronounced changes in cold pool parameter magnitude over time (Fig. 4b) than the RKW runs. For all grid configurations, cold pool intensities did not change by more than 1 m s^{-1} throughout the entirety of the model run, indicating that the simulated MCSs maintained a quasi-steady state after a period of rapid initial growth. There was almost no difference in cold pool intensity magnitude between 3 km-50 lev and 3 km-100 lev runs. Additionally, cold pool depths showed very few changes over time for all grid configurations (Fig. 5b). Similar to the results seen in RKW simulations, MC simulations with a 1-km Δx had slightly stronger cold pools (Figs. 4b and 6c,d) than MC simulations with a 3-km Δx. The general trend seen in Fig. 4 for stronger cold pools in 1-km runs than in 3-km runs in both the MC and RKW simulations is consistent with the trend found in the CM1 runs of Bryan and Morrison (2012) as horizontal grid spacing was changed from 4 to 1 km and the WRF runs of Weisman et al. (2023) that examined changes in horizontal grid spacing from 3 to 1 km. It should be noted, however, that Bryan and Morrison (2012) did not find the cold pool to continue to increase in intensity as horizontal grid spacing was refined further to 0.25 km, likely due to the development of resolved turbulence once grid spacing was refined to 0.25 km.

Composite reflectivity in the early hours (hours 4–6) of development (Figs. 2 and 3m–p) showed that RKW simulations produced a much more cohesive linear system than MC simulations. With the only factor differing between the simulations being the wind profile, it appears that the strength of the Weisman–Klemp *u*-wind multicell profile may have prevented cold pools from consolidating and growing larger; instead, the cold pools remained in a quasi-steady state throughout the model run in a manner more like a line of supercells. It was noted that differences between these runs with different shear profiles did not appear to depend on the horizontal grid spacing used (figure not shown). A qualitative analysis of the cold pool intensity for 1 km-100 lev RKW and MC runs supports this idea; the MC cold pools (Figs. 7e–h) were more diffuse and spread out with localized areas of stronger cold pools, while the RKW simulations (Figs. 8a–d) produced cold pools that were far more cohesive.

c. *Spatial examination of vertical velocity and potential temperature fields*

While simulations of MCSs with 1-km Δx produced stronger cold pools, the question remains as to what is happening

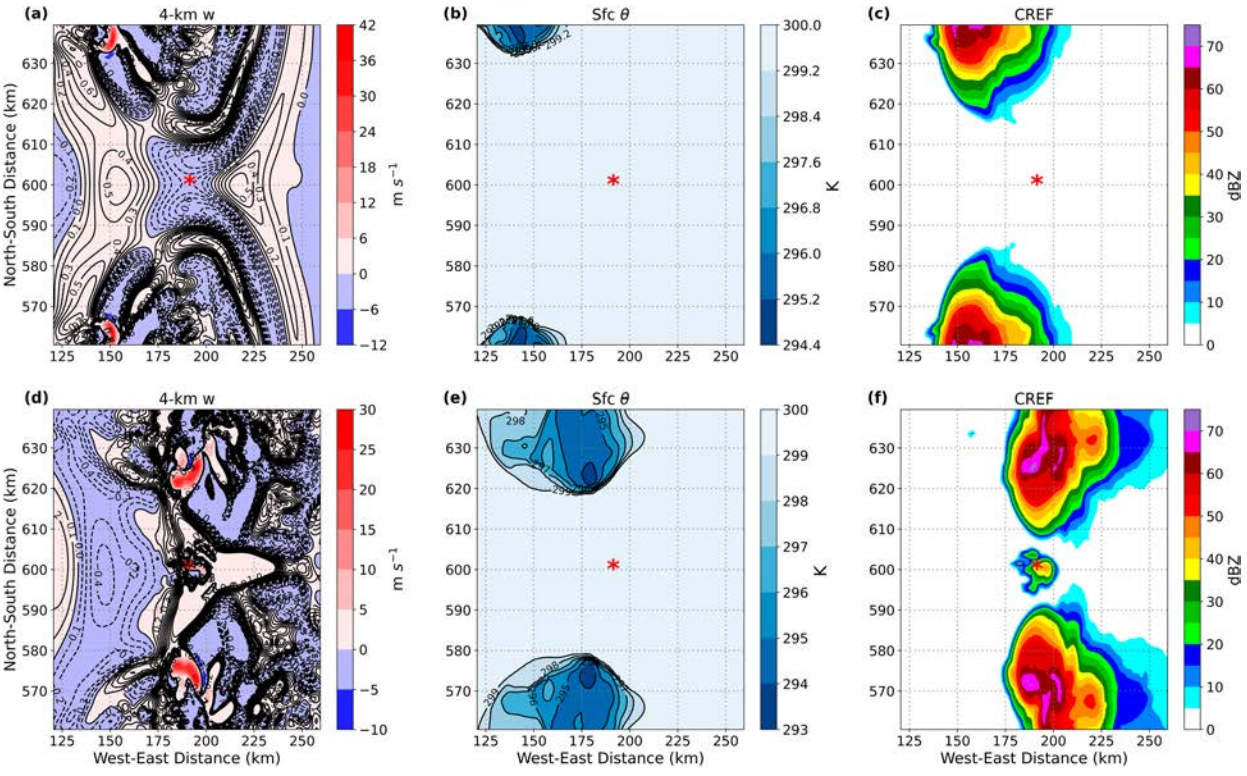

FIG. 8. Horizontal plots at 65 min into the 1 km-100 lev MC simulation of (a) vertical velocity (m s^{-1}) at a height of 4 km AGL, (b) surface potential temperature (K), (c) composite reflectivity (dBZ), and 90 min into the simulation for (d) vertical velocity (m s^{-1}) at a height of 4 km AGL, (e) surface potential temperature (K), and (f) composite reflectivity (dBZ). Solid contours in (a) and (d) indicate positive vertical velocity (upward motion); dashed contours indicate negative vertical velocity (downward motion). Note that color scales are not equal for the two vertical velocity panels; this is due to the washing out of gravity wave–scale vertical motion from the intrusion of significantly stronger vertical motions associated with convective updrafts from the northern and southern segments of the line. Additionally, color scales are not equal for potential temperature panels to better capture the extent of convective cold pools. The region shown is located in the northern portion of the line. A red asterisk in all panels indicates the location of convective initiation.

to promote linear organization in the clear regions between cells in the broken linear structure. Are cells forming more quickly or more frequently there due to stronger lift at the leading edge of the cold pool than in 3-km runs? If so, is the enhanced lift due to improved resolution alone, or a function also of the increased cold pool strength in the finer resolution runs? Or is new cell formation triggered by a different process altogether?

To answer these questions, a spatial examination of vertical velocity and potential temperature fields was performed. To accurately examine small-scale features, small sections of the domain centered on the areas of most interest were selected for more detailed analysis. These small sections were chosen where no convection was observed in 3-km simulations and where convection was observed in 1-km simulations. Multiple

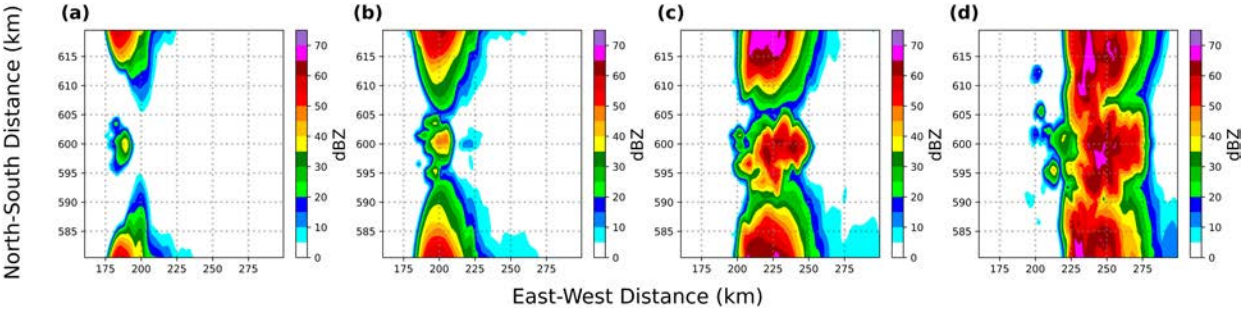

FIG. 9. Composite reflectivity (a) 90, (b) 100, (c) 115, and (d) 130 min into the 1 km-100 lev MC simulation showing the growth of a wave-induced convective cell and 0 incorporation of the cell into the linear system. The region shown is located in the northern portion of the line.

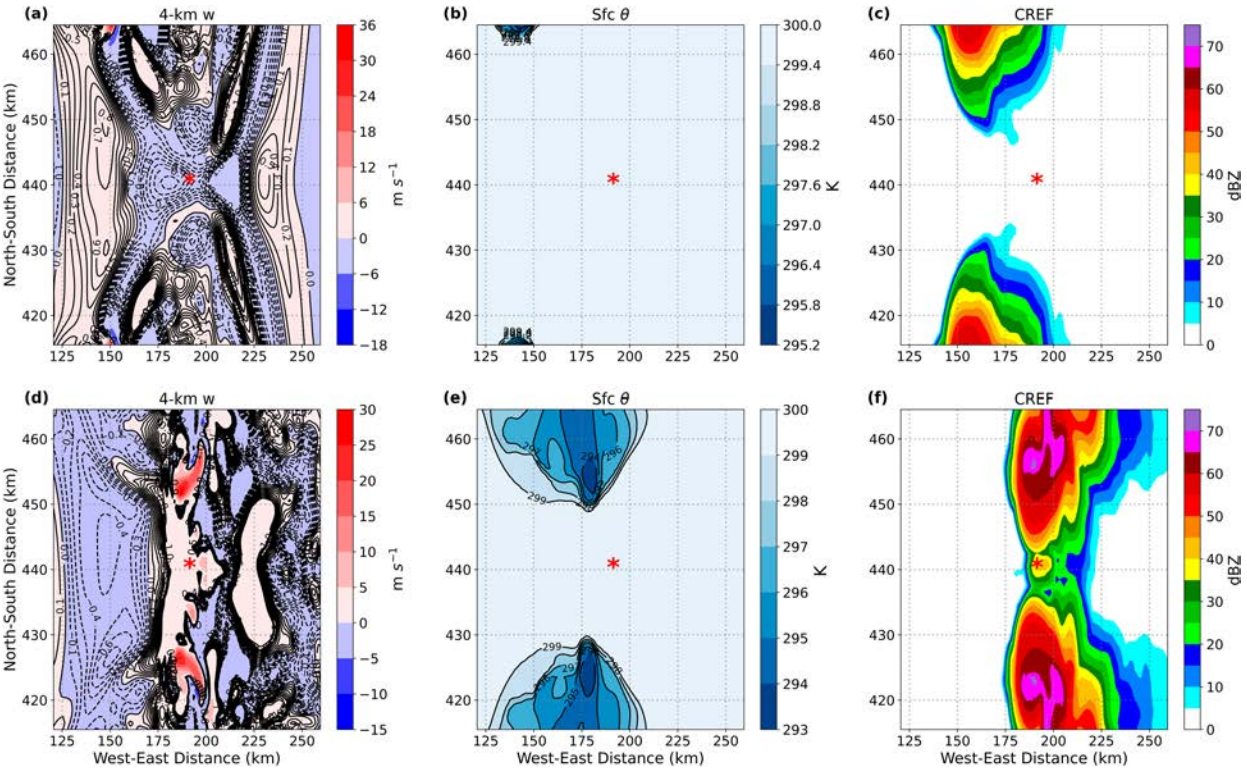

FIG. 10. As in Fig. 8, but showing the middle rather than the northern portion of the line.

levels were examined for vertical velocity to find small-scale features that led to upscale convective growth. Ultimately, the vertical velocity at a height of 4 km AGL was chosen as horizontal maps of vertical motion showed multiple instances of wavelike features being prominent at this level. To provide more clarity into potentially time-sensitive processes, MC simulations with grid configurations of 3 km-100 lev and 1 km-100 lev were rerun with a 5-min output time step for approximately 1.5 h over the window in which the clear region experienced convective initiation. Additionally, a 1 km-100 lev MC run was performed that turned off evaporative cooling to examine how the change impacted the reflectivity fields and upscale development, as well as the behavior of gravity waves. It was found that the differences in these fields due to the removal of evaporative cooling were minor, supporting the idea that cold pools were not the primary driver of convective organization and behavior.

As in prior work by Adams-Selin (2020a,b), gravity waves were observed in the present study's CM1 simulations, most distinctly at the 4-km level in the vertical velocity field in both multibubble (MB)-RKW and MC simulations. Wavelike features were most distinct in simulations with Δx of 1 km (Fig. 8) in clear regions between convective cells. Solid lines indicating positive vertical velocities and dashed lines indicating negative vertical velocities help to highlight these waves (Fig. 8a). These waves were found in multiple areas along the line, with Figs. 8 and 9 focusing on the northernmost portion of the line. Convective initiation occurred between 15 and 30 min after the waves passed through the convection-free area, indicating that the gravity waves may have destabilized the environment in this clear area such that a new convective cell was able to form with the small amount of lift provided by the waves. Also of note is that the cold pools (as indicated by the surface potential temperature) from the northern and southern ends of the MCS had not yet shown any significant development or maturity in the region undergoing convective initiation (Figs. 8b,e). This implies that the new convection was not triggered by lift directly associated with the cold pool. Continued tracking of the new convection reveals the congealing of the new cell into the main line (Fig. 9). As this wave-induced convection occurs in multiple clear regions in the broken line, the subsequent initiation, growth, and incorporation of these cells into the system result in a linear convective system.

Additional clear regions of the broken line were located and analyzed to see if gravity waves were present and seemed to play a role in new cell growth, likely through lift leading to destabilization. Two separate locations were found to have gravity waves present before and during new convective initiation in these clear regions. The middle portion of the line showed a similar pattern of new cell development seen in the northern portion of the line (Figs. 8 and 9), with wavelike features passing through the clear region between thunderstorms and new convection initiating between 15 and 30 min after wave passage (Figs. 10a,c,d,f). The new cell development occurred without any encroachment by cold pools in this clear

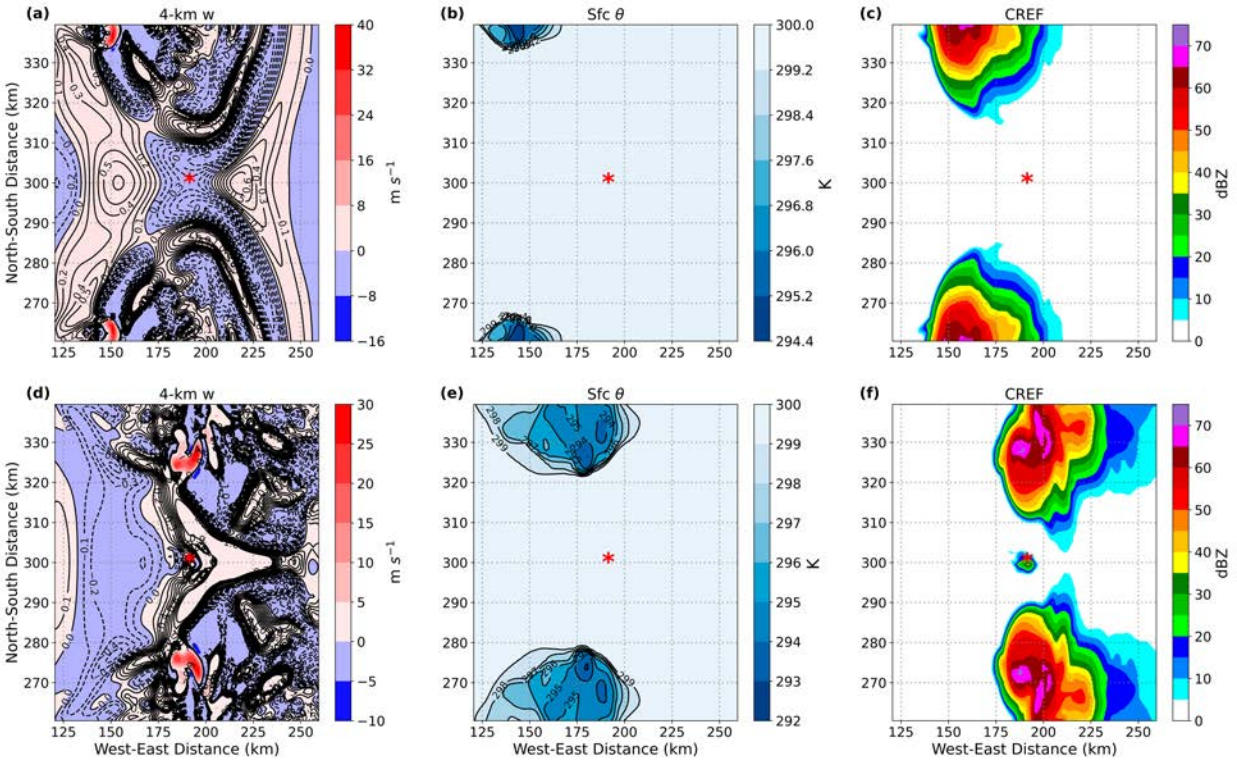

FIG. 11. As in Fig. 8, but for 65 and 90 min into the 1 km-100 lev MC simulation and for the southern part of the line.

region (Fig. 10e). The southern portion of the line also showed evidence of wavelike features in the clear region, with vertical motion strength being similar to the vertical motion strength seen in the middle and northern regions of the line (Figs. 11a,d). Additionally, cold pool encroachment in the southern clear region was slightly more pronounced, and convective updrafts were observed within the vertical velocity fields (Figs. 11a,b,d,e). Based on this, the mechanism for new cell initiation in the southern portion of the line was not as clear as it was in the northern and middle portions of the line. It may be possible that a combination of lift associated with cold pool encroachment and weak gravity wave activity are both responsible for the development of the new convective cells in that part of the line.

An analysis of the MB-RKW simulations with 1-km Δx was performed to see if gravity waves were also playing a role in new convective development. It was found that while there was some evidence of gravity waves progressing through the clear regions, distinct wavelike features were far less pronounced than those seen in the MC simulations (Figs. 12a,d). Additionally, convective cold pool encroachment was far greater in the MB-RKW simulations, which would indicate that stronger lift associated with these cold pools may be playing a larger part in the development of new cells (Fig. 12e).

The trend seen in the 1-km MC simulations was not as pronounced in the 3-km Δx MC simulations. The wavelike features observed in these simulations were notably weaker, with vertical velocities in the waves having maxima that were half as strong as those seen in MC simulations with 1-km Δx (Figs. 13a,d). Additionally, the new convection in the clear region in the 3-km simulations occurred approximately 1 h later than in the 1-km simulations. Cold pool encroachment was found to be more pronounced in the 3-km simulations, with the north and south edges of the cold pools nearly touching when convection occurred in the clear region, so that vertical forcing associated with the cold pool boundaries was likely the main forcing mechanism for initiation of new convection in MC simulations with 3-km Δx.

This trend for initiation in the MC simulations with 3-km Δx to be more obviously forced by lift at the edge of cold pools was observed at more than one location in the convective line. In these locations, wavelike structures were even notably weaker, and the cold pool extent was much closer to the site of new convective development in the clear regions (Figs. 14a,d,g,h). These trends were also found in MB-RKW simulations with 3-km Δx. Wavelike behavior was observed in these simulations, but the waves were notably more disorganized in the 3-km run when compared to those seen in the MC simulations with 1-km Δx (Fig. 10a). Additionally, new convection in the clear region was not observed until the north and south cold pools had merged (Figs. 15e,f,h,i). Since weak wavelike features were observed in these 3-km simulations, it may be the case that although the initiation of new convection leading to upscale growth into linear morphologies in the 3-km runs was primarily driven by cold pool dynamics, weak gravity waves did play a minor role. However, in 1-km simulations, it appears that gravity waves were a

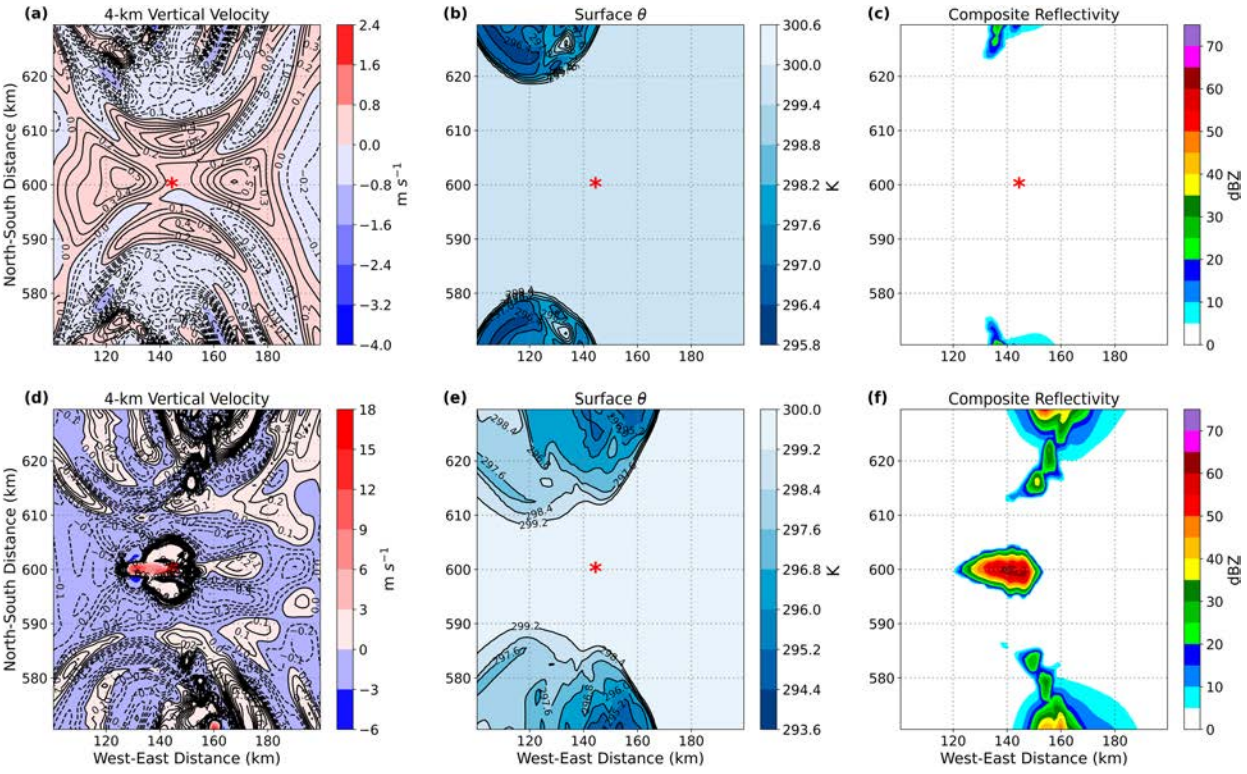

FIG. 12. As in Fig. 8, but for 90 and 120 min into the 1 km-100 lev MB-RKW simulation, showing the northern portion of the line.

significant factor in the cause of convective initiation and its earlier occurrence. It should be noted that while gravity waves appeared to play a major role in convective initiation in 1-km simulations, the influence of vertical forcing induced by convective cold pools cannot be ruled out as a contributing factor.

To confirm that these bands of vertical motion at 4 km AGL were gravity waves in 1-km simulations, wave speeds were calculated for these features with the 5-min model output. Multiple portions of these bands were selected and followed over their observable lifespan to provide an average motion for these features. It was found for 1 km-100 lev MC simulations that these gravity waves were propagating at an average speed of 33 m s^{-1}. Table 1 indicates this wave speed is consistent with a second-order gravity wave. As found in Adams-Selin (2020a), gravity waves of second order are generated by cooling from midlevels to the surface, and they act to destabilize the atmosphere in the regions they pass over.

4. Conclusions

MCSs produced by 1-km RKW simulations appeared more cohesive in their linear structure than the MCSs produced by 3-km RKW simulations. The number of vertical levels used in RKW simulations did not appear to profoundly impact the MCS structure. All MCSs produced by RKW simulations had trailing stratiform precipitation regions for all grid configurations. Conversely, MCSs produced by MC simulations all had somewhat broken linear structures by maturity. MC simulations with horizontal grid spacings of 1 km produced MCSs with slightly more cohesive structures than MC simulations with horizontal grid spacings of 3 km. MC simulations with 100 vertical levels produced MCSs with slightly more contiguous linear structures than MC simulations with 50 vertical levels. All MCSs produced by MC simulations had leading stratiform precipitation regions for all grid configurations likely due to the strength of the Weisman–Klemp multicell u-wind profile.

Cold pool intensities were found to be stronger in simulations with 1-km horizontal grid spacing in both RKW and MC simulations than in these simulations with 3-km horizontal grid spacing. RKW runs produced cold pools that steadily increased in intensity and depth over time, while MC runs produced cold pools that maintained a quasi-steady state in both intensity and depth. This quasi-steady state was likely the result of the wind profile chosen; the multicell wind profile has both stronger winds and wind shear over a deeper layer than the RKW wind profile, and as a result, there is likely some disruption of cold pool organization and strengthening.

It was found that MC and, to a lesser extent, RKW simulations with a 1-km Δx produce MCSs that grow upscale from cellular morphologies to linear morphologies with forcing and destabilization that is primarily induced by convectively generated second-order gravity waves. While vertical forcing from convectively generated cold pools may play a role in these simulations, the idea that cells form more quickly due to

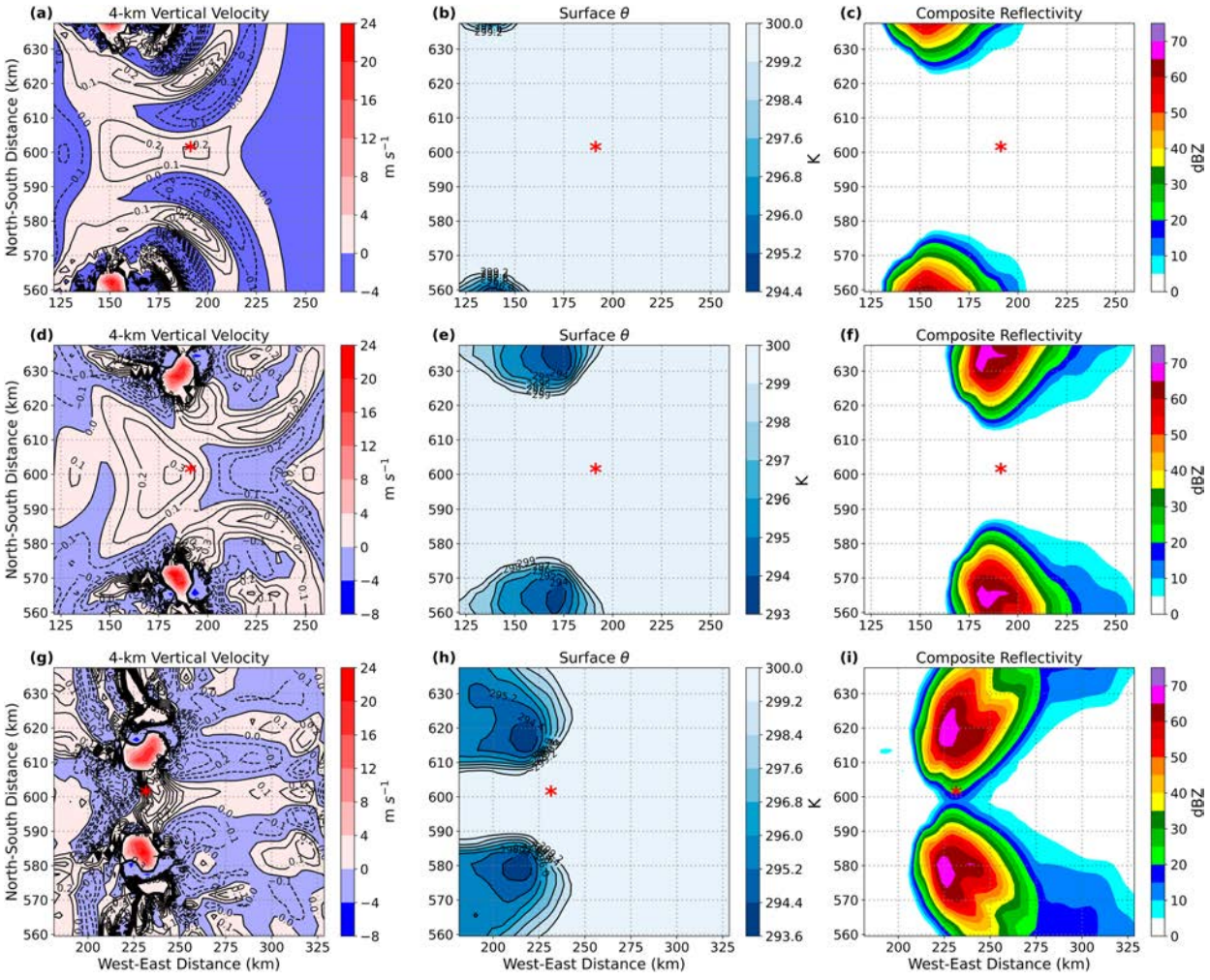

FIG. 13. As in Fig. 8, but for the 3 km-100 lev MC simulation, 65, 90, and 125 min into the simulation showing the northern portion of the line.

stronger lift from cold pools was unsupported by the data in these simulations. Additionally, a 1 km-100 lev run with the multicell wind profile was performed with evaporative cooling turned off. Results showed that turning off evaporative cooling had minimal impact on reflectivity fields, the evolution of the convective system, and the behavior of gravity waves. This also supported the idea that cold pools were not the primary driver of convective organization and behavior. This is true even considering the fact that cold pool intensities were found to be stronger in 1-km Δx simulations for both RKW and MC configurations. In some portions of the line, the edges of the cold pools were approximately 25 km from the newly generated convection, too far to be the causative mechanism for new convection. However, some portions of the line did show cold pool edges that were located approximately 5 km from the new convection, and it may be that the combination of forcing from both the gravity waves and the cold pools is the root cause of the new convection in these locations.

In contrast, in RKW and MC simulations with a 3-km Δx, new convection in clear regions was triggered primarily by the collision of cold pools and the increased vertical motion associated with the collisions. Ascent related to gravity waves was much weaker and likely not the driving force behind convective initiation and subsequent linear growth. As far as we know, this result has not been found in prior works, and it indicates that the mechanism by which simulated MCSs grow upscale may be highly dependent on horizontal grid spacing, meaning that finer horizontal grid spacing may be needed to properly resolve dynamic and thermodynamic processes that directly lead to upscale convective growth and influence storm morphology evolution.

It may also be the case that the mechanism by which simulated MCSs grow upscale may also depend on the wind profile present in the simulation. It was noted that RKW simulations produced weaker gravity waves than MC simulations for both 1 and 3 km Δx. The RKW wind profile is much weaker in magnitude than the multicell wind profile,

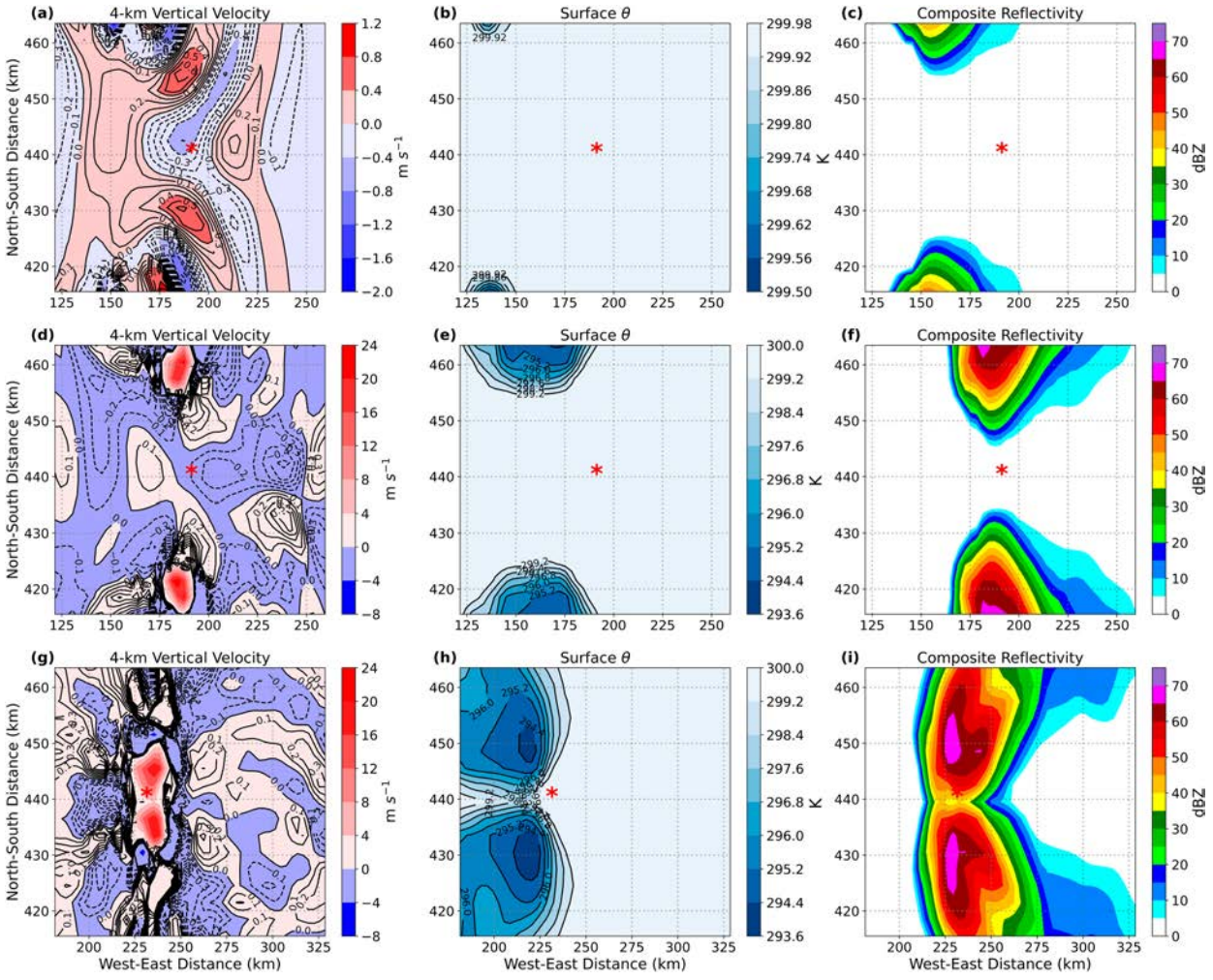

FIG. 14. As in Fig. 8, but for the 3 km-100 lev MC simulation, 65, 90, and 120 min into the simulation showing the middle portion of the line.

and the lack of robust wind shear in the RKW profile may inhibit the production of stronger gravity waves. This is supported by the finding in Groff et al. (2021) that environments with strong vertical wind shear are capable of supporting gravity waves with enough strength to cause new convection ahead of the MCS and to support preexisting convection.

To answer the questions posed in section 3c of the present work, new cell formation as a result of stronger lift at the leading edge of cold pools in 1-km runs when compared to 3-km runs was not supported by the CM1 simulations. While the improvements in resolution at 1-km grid spacings did result in stronger cold pools, the idea that the stronger cold pools provide enhanced lift leading to new cell formation was also unsupported. It was found that new cell formation in multiple cases in the 1-km runs was the result of a different process, enhanced lift provided by convectively generated gravity waves. Thus, it is likely that new convection in the finer grid spacing runs is initiated by a combination of gravity wave and cold pool forcing. Future work should explore the individual roles of these two mechanisms in further detail and with a wider variety of background thermodynamic and wind shear conditions.

In addition, future work should use fine spatial observations from field projects to determine if a similar process happens in nature; that is, upscale growth into lines is facilitated by new cells forming between existing cells due to gravity waves well away from lift along cold pool boundaries. Additional modeling work should examine the sensitivity of the results presented here to changes in the relative humidity of the lower troposphere and should focus on the sensitivity of gravity waves to various factors since Adams-Selin (2020b) found that gravity waves are sensitive in some ways to microphysical schemes. Related to this, the sensitivity of the results to the process used to initiate convection should be examined, since it is possible that the warm bubbles used in the present study may themselves generate gravity waves. Additionally, cold pool sensitivities to changes in microphysical schemes should be examined. Finally, it would be of interest to examine if subsequent refinement of horizontal grid spacings to values less than 1 km changes the depiction of gravity waves and the

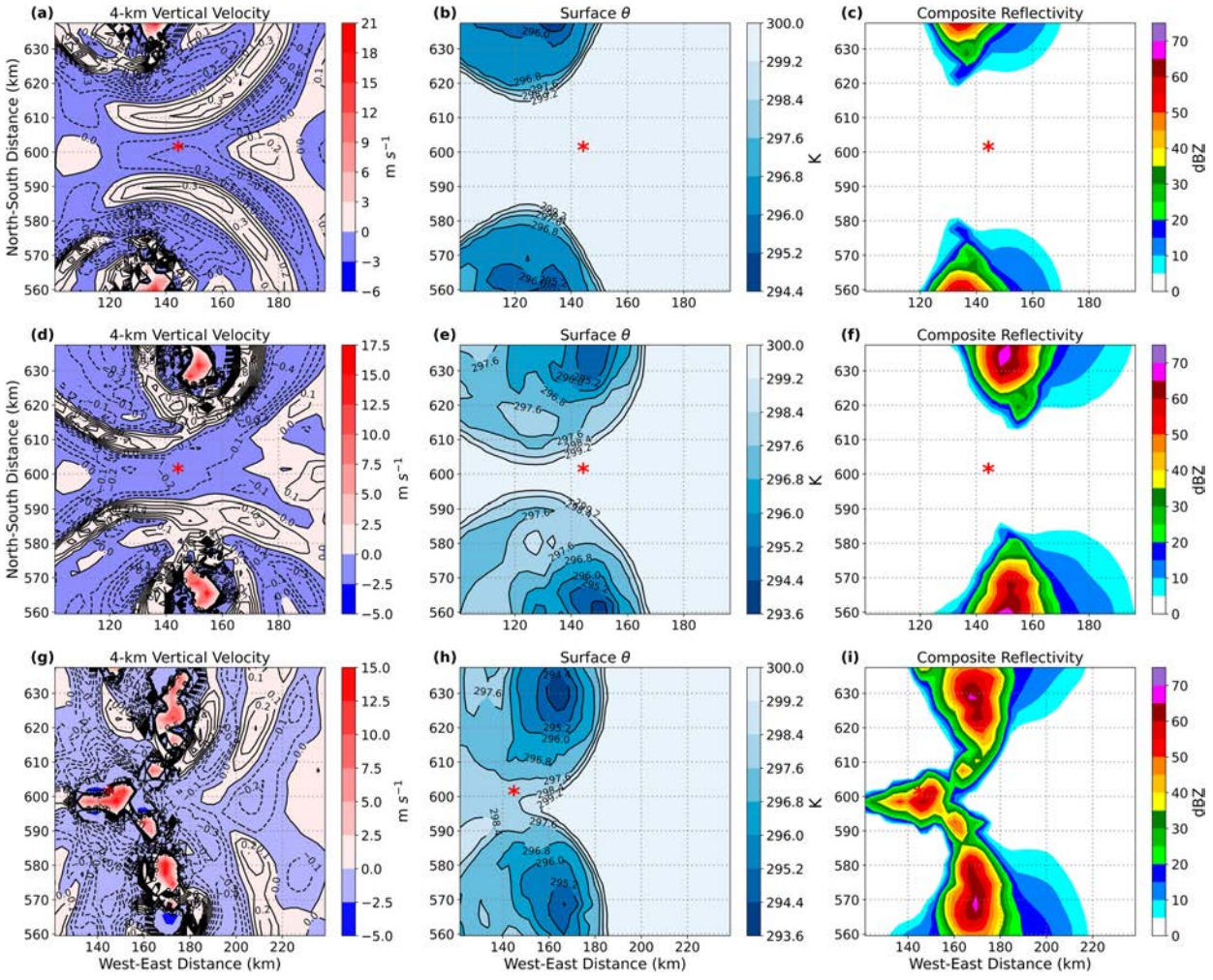

FIG. 15. As in Fig. 8, but for the 3 km-100 lev MB-RKW simulation, 90, 120, and 150 min into the simulation showing the northern portion of the line.

role they play in upscale convective growth compared to what was found here for 1-km grid spacing.

Acknowledgments. This research was supported by National Science Foundation Grants AGS2022888 and AGS2350205. Acknowledgment is given to the high-performance computing support from Cheyenne (https://doi.org/10.5065/D6RX99HX) provided by NCAR's Computational and Information Systems Laboratory, sponsored by the National Science Foundation. Gratitude is extended to Jonathan Thielen for his assistance in the development of Python codes for data analysis and Brian Squitieri for help throughout the research process. The paper was significantly improved by the constructive comments of three reviewers.

Data availability statement. The data that support the findings of this work are stored on a server at Iowa State University and are available from the corresponding author upon request.

REFERENCES

Adams-Selin, R. D., 2020a: Impact of convectively generated low-frequency gravity waves on evolution of mesoscale convective systems. *J. Atmos. Sci.*, **77**, 3441–3460, https://doi.org/10.1175/JAS-D-19-0250.1.

——, 2020b: Sensitivity of MCS low-frequency gravity waves to microphysical variations. *J. Atmos. Sci.*, **77**, 3461–3477, https://doi.org/10.1175/JAS-D-19-0347.1.

Ashley, W. S., T. L. Mote, P. G. Dixon, S. L. Trotter, E. J. Powell, J. D. Durkee, and A. J. Grundstein, 2003: Distribution of mesoscale convective complex rainfall in the United States. *Mon. Wea. Rev.*, **131**, 3003–3017, https://doi.org/10.1175/1520-0493(2003)131%3C3003:DOMCCR%3E2.0.CO;2.

Bryan, G. H., and J. M. Fritsch, 2002: A benchmark simulation for moist nonhydrostatic numerical models. *Mon. Wea. Rev.*, **130**, 2917–2928, https://doi.org/10.1175/1520-0493(2002)130<2917:ABSFMN>2.0.CO;2.

——, and H. Morrison, 2012: Sensitivity of a simulated squall line to horizontal resolution and parameterization of microphysics.

Mon. Wea. Rev., **140**, 202–225, https://doi.org/10.1175/MWR-D-11-00046.1.

——, J. C. Wyngaard, and J. M. Fritsch, 2003: Resolution requirements for the simulation of deep moist convection. *Mon. Wea. Rev.*, **131**, 2394–2416, https://doi.org/10.1175/1520-0493(2003)131<2394:RRFTSO>2.0.CO;2.

Carbone, R. E., and J. D. Tuttle, 2008: Rainfall occurrence in the U.S. warm season: The diurnal cycle. *J. Climate*, **21**, 4132–4146, https://doi.org/10.1175/2008JCLI2275.1.

Carlberg, B. R., W. A. Gallus Jr., and K. J. Franz, 2018: A preliminary examination of WRF ensemble prediction of convective mode evolution. *Wea. Forecasting*, **33**, 783–798, https://doi.org/10.1175/WAF-D-17-0149.1.

Clark, A. J., W. A. Gallus Jr., M. Xue, and F. Kong, 2010a: Convection-allowing and convection-parameterizing ensemble forecasts of a mesoscale convective vortex and associated severe weather environment. *Wea. Forecasting*, **25**, 1052–1081, https://doi.org/10.1175/2010WAF2222390.1.

——, ——, and M. L. Weisman, 2010b: Neighborhood-based verification of precipitation forecasts from convection-allowing NCAR WRF model simulations and the operational NAM. *Wea. Forecasting*, **25**, 1495–1509, https://doi.org/10.1175/2010WAF2222404.1.

——, and Coauthors, 2011: Probabilistic precipitation forecast skill as a function of ensemble size and spatial scale in a convection-allowing ensemble. *Mon. Wea. Rev.*, **139**, 1410–1418, https://doi.org/10.1175/2010MWR3624.1.

Coniglio, M. C., and D. J. Stensrud, 2001: Simulation of a progressive derecho using composite initial conditions. *Mon. Wea. Rev.*, **129**, 1593–1616, https://doi.org/10.1175/1520-0493(2001)129%3C1593:SOAPDU%3E2.0.CO;2.

——, J. Y. Hwang, and D. J. Stensrud, 2010: Environmental factors in the upscale growth and longevity of MCSs derived from Rapid Update Cycle analyses. *Mon. Wea. Rev.*, **138**, 3514–3539, https://doi.org/10.1175/2010MWR3233.1.

Done, J., C. A. Davis, and M. Weisman, 2004: The next generation of NWP: Explicit forecasts of convection using the weather research and forecasting (WRF) model. *Atmos. Sci. Lett.*, **5**, 110–117, https://doi.org/10.1002/asl.72.

French, A. J., and M. D. Parker, 2012: Observations of mergers between squall lines and isolated supercell thunderstorms. *Wea. Forecasting*, **27**, 255–278, https://doi.org/10.1175/WAF-D-11-00058.1.

Fritsch, J. M., R. J. Kane, and C. R. Chelius, 1986: The contribution of mesoscale convective weather systems to the warm-season precipitation in the United States. *J. Climate Appl. Meteor.*, **25**, 1333–1345, https://doi.org/10.1175/1520-0450(1986)025<1333:TCOMCW>2.0.CO;2.

Gallo, B. T., and Coauthors, 2017: Breaking new ground in severe weather prediction: The 2015 NOAA/Hazardous Weather Testbed Spring Forecasting Experiment. *Wea. Forecasting*, **32**, 1541–1568, https://doi.org/10.1175/WAF-D-16-0178.1.

Gallus, W. A., Jr., N. A. Snook, and E. V. Johnson, 2008: Spring and summer severe weather reports over the Midwest as a function of convective mode: A preliminary study. *Wea. Forecasting*, **23**, 101–113, https://doi.org/10.1175/2007WAF2006120.1.

Geerts, B., and Coauthors, 2017: The 2015 Plains Elevated Convection at Night field project. *Bull. Amer. Meteor. Soc.*, **98**, 767–786, https://doi.org/10.1175/BAMS-D-15-00257.1.

Groff, F. P., R. D. Adams-Selin, and R. S. Schumacher, 2021: Response of MCS low-frequency gravity waves to vertical wind shear and nocturnal thermodynamic environments. *J. Atmos. Sci.*, **78**, 3889–3908, https://doi.org/10.1175/JAS-D-20-0208.1.

Haberlie, A. M., and W. S. Ashley, 2019: A radar-based climatology of mesoscale convective systems in the United States. *J. Climate*, **32**, 1591–1606, https://doi.org/10.1175/JCLI-D-18-0559.1.

Hiris, Z. A., and W. A. Gallus Jr., 2021: On the relationship of cold pool and bulk shear magnitudes on upscale convective growth in the Great Plains of the United States. *Atmosphere*, **12**, 1019, https://doi.org/10.3390/atmos12081019.

Hobbs, P. V., and J. M. Wallace, 2006: *Atmospheric Science: An Introductory Survey*. 2nd ed. Academic Press, 504 pp.

James, R. P., J. M. Fritsch, and P. M. Markowski, 2005: Environmental distinctions between cellular and slabular convective lines. *Mon. Wea. Rev.*, **133**, 2669–2691, https://doi.org/10.1175/MWR3002.1.

Janjić, Z. I., 1990: The step-mountain coordinate: Physical package. *Mon. Wea. Rev.*, **118**, 1429–1443, https://doi.org/10.1175/1520-0493(1990)118<1429:TSMCPP>2.0.CO;2.

——, 1994: The Step-Mountain Eta Coordinate Model: Further developments of the convection, viscous sublayer, and turbulence closure schemes. *Mon. Wea. Rev.*, **122**, 927–945, https://doi.org/10.1175/1520-0493(1994)122<0927:TSMECM>2.0.CO;2.

——, J. P. Gerrity Jr., and S. Nickovic, 2001: An alternative approach to nonhydrostatic modeling. *Mon. Wea. Rev.*, **129**, 1164–1178, https://doi.org/10.1175/1520-0493(2001)129<1164:AAATNM>2.0.CO;2.

Jirak, I. L., and W. R. Cotton, 2007: Observational analysis of the predictability of mesoscale convective systems. *Wea. Forecasting*, **22**, 813–838, https://doi.org/10.1175/WAF1012.1.

Junker, N. W., R. S. Schneider, and S. L. Fauver, 1999: A study of heavy rainfall events during the great Midwest flood of 1993. *Wea. Forecasting*, **14**, 701–712, https://doi.org/10.1175/1520-0434(1999)014<0701:ASOHRE>2.0.CO;2.

Maddox, R. A., 1980: Mesoscale convective complexes. *Bull. Amer. Meteor. Soc.*, **61**, 1374–1387, https://doi.org/10.1175/1520-0477(1980)061<1374:MCC>2.0.CO;2.

——, D. M. Rodgers, and K. W. Howard, 1982: Mesoscale convective complexes over the United States during 1981—Annual summary. *Mon. Wea. Rev.*, **110**, 1501–1514, https://doi.org/10.1175/1520-0493(1982)110<1501:MCCOTU>2.0.CO;2.

Parker, M. D., 2021: Self-organization and maintenance of simulated nocturnal convective systems from PECAN. *Mon. Wea. Rev.*, **149**, 999–1022, https://doi.org/10.1175/MWR-D-20-0263.1.

——, B. S. Borchardt, R. L. Miller, and C. L. Ziegler, 2020: Simulated evolution and severe wind production by the 25–26 June 2015 nocturnal MCS from PECAN. *Mon. Wea. Rev.*, **148**, 183–209, https://doi.org/10.1175/MWR-D-19-0072.1.

Rotunno, R., J. B. Klemp, and M. L. Weisman, 1988: A theory for strong, long-lived squall lines. *J. Atmos. Sci.*, **45**, 463–485, https://doi.org/10.1175/1520-0469(1988)045%3C0463:ATFSLL%3E2.0.CO;2.

Schwartz, C. S., and R. A. Sobash, 2019: Revisiting sensitivity to horizontal grid spacing in convection-allowing models over the central and eastern United States. *Mon. Wea. Rev.*, **147**, 4411–4435, https://doi.org/10.1175/MWR-D-19-0115.1.

——, G. S. Romine, K. R. Fossell, R. A. Sobash, and M. L. Weisman, 2017: Toward 1-km ensemble forecasts over large domains. *Mon. Wea. Rev.*, **145**, 2943–2969, https://doi.org/10.1175/MWR-D-16-0410.1.

Snively, D. V., and W. A. Gallus Jr., 2014: Prediction of convective morphology in near-cloud-permitting WRF model simulations.

Wea. Forecasting, **29**, 130–149, https://doi.org/10.1175/WAF-D-13-00047.1.

Squitieri, B. J., and W. A. Gallus Jr., 2016: WRF forecasts of Great Plains nocturnal low-level jet-driven MCSs. Part II: Differences between strongly and weakly forced low-level jet environments. *Wea. Forecasting*, **31**, 1491–1510, https://doi.org/10.1175/WAF-D-15-0150.1.

——, and ——, 2020: On the forecast sensitivity of MCS cold pools and related features to horizontal grid spacing in convection-allowing WRF simulations. *Wea. Forecasting*, **35**, 325–346, https://doi.org/10.1175/WAF-D-19-0016.1.

——, and ——, 2022a: On the changes in convection-allowing WRF forecasts of MCS evolution due to decreases in model horizontal and vertical grid spacing. Part I: Changes in cold pool evolution. *Wea. Forecasting*, **37**, 1903–1923, https://doi.org/10.1175/WAF-D-22-0041.1.

——, and ——, 2022b: On the changes in convection-allowing WRF forecasts of MCS evolution due to decreases in model horizontal and vertical grid spacing. Part II: Impacts on QPFs. *Wea. Forecasting*, **37**, 1925–1940, https://doi.org/10.1175/WAF-D-22-0042.1.

Stensrud, D. J., and J. M. Fritsch, 1994: Mesoscale convective systems in weakly forced large-scale environments. Part III: Numerical simulations and implications for operational forecasting. *Mon. Wea. Rev.*, **122**, 2084–2104, https://doi.org/10.1175/1520-0493(1994)122%3C2084:MCSIWF%3E2.0.CO;2.

Thielen, J. E., and W. A. Gallus Jr., 2019: Influences of horizontal grid spacing and microphysics on WRF forecasts of convective morphology evolution for nocturnal MCSs in weakly forced environments. *Wea. Forecasting*, **34**, 1495–1517, https://doi.org/10.1175/WAF-D-18-0210.1.

Thompson, G., P. R. Field, R. M. Rasmussen, and W. D. Hall, 2008: Explicit forecasts of winter precipitation using an improved bulk microphysics scheme. Part II: Implementation of a new snow parameterization. *Mon. Wea. Rev.*, **136**, 5095–5115, https://doi.org/10.1175/2008MWR2387.1.

Weisman, M. L., 1992: The role of convectively generated rear-inflow jets in the evolution of long-lived mesoconvective systems. *J. Atmos. Sci.*, **49**, 1826–1847, https://doi.org/10.1175/1520-0469(1992)049<1826:TROCGR>2.0.CO;2.

——, and J. B. Klemp, 1982: The dependence of numerically simulated convective storms on vertical wind shear and buoyancy. *Mon. Wea. Rev.*, **110**, 504–520, https://doi.org/10.1175/1520-0493(1982)110<0504:TDONSC>2.0.CO;2.

——, W. C. Skamarock, and J. B. Klemp, 1997: The resolution dependence of explicitly modeled convective systems. *Mon. Wea. Rev.*, **125**, 527–548, https://doi.org/10.1175/1520-0493(1997)125<0527:TRDOEM>2.0.CO;2.

——, C. Davis, W. Wang, K. W. Manning, and J. B. Klemp, 2008: Experiences with 0–36-h explicit convective forecasts with the WRF-ARW model. *Wea. Forecasting*, **23**, 407–437, https://doi.org/10.1175/2007WAF2007005.1.

——, K. W. Manning, R. A. Sobash, and C. S. Schwartz, 2023: Simulations of severe convective systems using 1- versus 3-km grid spacing. *Wea. Forecasting*, **38**, 401–423, https://doi.org/10.1175/WAF-D-22-0112.1.